

Anisotropic membrane curvature sensing by antibacterial peptides

Jordi Gómez-Llobregat,^{1,*} Federico Elías-Wolff,^{1,†} and Martin Lindén^{2,‡}

¹*Center for biomembrane research, Department of Biochemistry and Biophysics, Stockholm University, SE-106 91 Stockholm, Sweden*

²*Department of Cell and Molecular Biology, Uppsala University, Box 596, 751 24 Uppsala, Sweden*

(Dated: June 18, 2022)

Many proteins and peptides have an intrinsic capacity to sense and induce membrane curvature, and play crucial roles for organizing and remodeling cell membranes. However, the molecular driving forces behind these processes are not well understood. Here, we describe a new approach to study curvature sensing, by simulating the direction-dependent interactions of single molecules with a buckled lipid bilayer. We analyze three antimicrobial peptides, a class of membrane-associated molecules that specifically target and destabilize bacterial membranes, and find qualitatively different sensing characteristics that would be difficult to resolve with other methods. These findings challenge existing theories of hydrophobic insertion, and provide new insights into the microscopic mechanisms of antimicrobial peptides, which might aid the development of new antibiotics. Our approach is generally applicable to a wide range of curvature sensing molecules, and our results provide strong motivation to develop new experimental methods to track position and orientation of membrane proteins.

INTRODUCTION

Curvature sensing and generation by membrane proteins and lipids is ubiquitous in cell biology, for example to maintain highly curved shapes of organelles, or drive membrane remodeling processes [1]. Membrane curvature sensing occurs if a molecule's binding energy depends on the local curvature [2]. For proteins, the presence of multiple conformations with different curvature preferences can couple protein function to membrane curvature [3], with interesting but largely unexplored biological implications.

Curvature sensing by lipids is often rationalized by a lipid shape factor, classifying lipids as 'cylindrical' or 'conical' when they prefer flat or curved membranes, respectively [1, 2]. Membrane proteins offer a wider range of sizes, shapes, and anchoring mechanisms [4], and thus potentially more diverse sensing mechanisms. In particular, shape asymmetry implies that the binding energy depends on the protein orientation in the membrane plane [5], and thus cannot be a function of only mean and Gaussian curvature, which are rotationally invariant. This calls for more complex descriptions, and one natural extension is to model the binding energy in terms of the local curvature tensor C_{ij} in a frame rotating with the protein [5–11], which allows different curvature preferences in different directions. For example, a preference for longitudinal curvature is generally associated with proteins that are curved in this direction, such as BAR domains [12, 13], whereas amphipatic helices [14] are expected to sense transverse curvature, since their insertion into the membrane-water interface is en-

ergetically favored if the membrane curves away in the transverse direction [15, 16].

Anisotropic curvature sensing is potentially complex, and theoretical investigations have demonstrated a wide range of qualitative behavior in local curvature models [5–11], but the models have not been rigorously tested. In principle, the curvature-dependent binding energy landscape $E(C_{ij})$ could be determined by measuring the Boltzmann distribution of protein configurations on curved membranes of known shape. However, current experimental techniques track only protein positions [17–23], and hence orientational information is averaged out. Here, we report the first data set tracking both position and orientation of single molecules, using a new computational approach based on simulated membrane buckling.

The method is applied to three amphipatic antimicrobial model peptides. Antimicrobial peptides can disrupt bacterial membranes at concentrations above some critical threshold. Many antimicrobial peptides are believed to work by mediating membrane pore formation via mechanisms that are not well understood [24]. The ability to stabilize highly curved pore structures suggests an intrinsic preference for curved surfaces. To explore different sensing characteristics, we choose peptides with different lengths and shapes, shown in Fig. 1: magainin, which is found in the skin of the African clawed frog [25], melittin, an active component in bee venom [26], and LL-37, a peptide derived from the human protein cathelicidin which is involved in the innate immune defense system [27].

Our method uses simulated membrane buckling to sample the unconstrained interaction of single biomolecules with a range of membrane curvatures, and extends previous simulation studies of buckling mechanics [28, 29], curvature-dependent folding and binding of amphipatic helices [30], and lipid partitioning [31]. We obtain joint distributions of peptide positions and orientations that yield new biophysical insights about curva-

* jordi.gomez@dbb.su.se

† federico.elias.wolff@dbb.su.se

‡ martin.linden@icm.uu.se

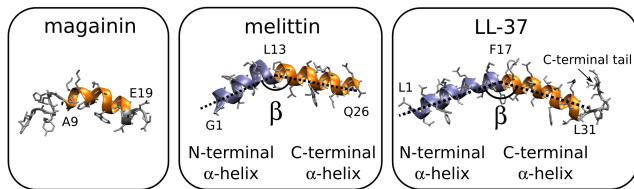


FIG. 1. (Color online) Structures of magainin [32], melittin [33] and LL-37 [31]. The melittin and LL-37 structures contain two α -helices that form an angle β (not the same for both structures). The α -helices used in the analysis are colored in blue (N-terminal) and orange (C-terminal), with the limiting amino acids labeled on the structure. Side chain and non-helical residues are colored in gray.

ture sensing. The three model peptides display similar rotation-averaged curvature preferences but differ in orientational preferences, which demonstrates the value of directional information. The asymmetry of the position-orientational distributions challenges continuum models of amphipatic helices as cylindrical membrane inclusions [15, 16]. We speculate that such asymmetry is important for certain modes of antibacterial activity, and argue that it might be common also for larger curvature sensing proteins. Finally, our theoretical analysis reveals a fundamental limitation in the ability to characterize curvature sensing mechanisms from assays with zero Gaussian curvature. These results motivate efforts to track positions and orientations of membrane proteins experimentally, and to develop assays with more complex geometry.

METHODS

To study curvature sensing by single peptides, we simulate their interactions with a buckled membrane using the coarse-grained Martini model [35], and track their position and orientation, as shown in Fig. 2. On a microscopic level, curvature sensing by amphipatic helices is associated with the density and size of bilayer surface defects [30, 36], which are well described by the Martini model [37].

a. Simulation parameters We performed molecular dynamics simulations using Gromacs 4.6.1 [38], and the coarse-grained Martini force-field with polarizable water model [35, 39, 40], and a relative dielectric constant of 2.5 (as recommended [40]). We used standard lipid parameters for 1-palmitoyl-2-oleoyl-sn-glycero-3-phosphocholine (POPC) [41], 1-palmitoyl-2-oleoyl phosphatidylglycerol (POPG) [42], and peptides [43]. The peptide structures for magainin (PDB ID:1DUM), melittin (PDB ID:2MLT), and LL-37 (PDB ID: 2K6O) were obtained from the Protein Data Bank, and coarse-grained with the martinize script provided by the MARTINI developers. Constant temperature was maintained with the velocity rescaling thermostat [44] with a 1.0 ps time constant, and pressure was controlled with the Berendsen

barostat [45] using a time constant of 12 ps and a compressibility of $3 \times 10^{-4} \text{ bar}^{-1}$. Peptide (when present), lipids and solvent were coupled separately to the temperature bath. Coulomb interactions were modeled with the particle mesh Ewald method [46] setting the real-space cut-off to 1.4 nm and the Fourier grid spacing to 0.12 nm. Lennard-Jones interactions were shifted to zero between 0.9 and 1.2 nm. A time step of 25 fs was used in all simulations.

b. System assembly and membrane buckling We assembled and equilibrated three rectangular ($L_x = 2L_y$) bilayer patches of 1024 lipids each, with 80% POPC and 20% POPG, solvated with ~ 21000 coarse-grained water beads and neutralized with sodium ion beads. POPG is negatively charged, which promotes peptide binding. These patches were equilibrated for 25 ns in an NPT ensemble at 300 K and 1 bar, with pressure coupling applied semi-isotropically.

After equilibration, all systems were laterally compressed in the x direction by a factor $\gamma = (L - L_x)/L = 0.2$, where L is the linear size of the flat system, and L_x the size of the compressed simulation box, in the x direction. This was done by scaling all x-coordinates, and the box size L_x , by a factor $1 - \gamma = 0.8$ at the end of the equilibration run, yielding $L_x = 20.88, 20.81$ and 20.89 nm for the three patches, respectively. After rescaling, the compressibilities were set to 0 in the x and y directions to keep the system size constant in those directions for subsequent simulations. Pressure coupling was then applied anisotropically in the z direction only. We then performed an energy minimization and a short equilibration run (25 ns) to let the bilayer buckle.

Next, we added one peptide to each system, using the three independent patches to create three independent replicas for each peptide. The peptide was initially placed about 3 nm above the membrane surface, but quickly attached to the bilayer. After the binding event, we equilibrated the system for another 5 μs before starting a production run of 15 μs , where we collected data every 5 ns. All peptides remained essentially parallel to the membrane surface as expected, in agreement with experimental results for low peptide concentrations [32, 33, 47, 48].

c. Membrane alignment and peptide tracking The buckled membrane profile diffuses as a traveling wave the simulation (movie S1), but curvature sensing by a peptide is reflected in its distribution relative to the buckled shape. Hence, the buckled configurations must be aligned in order to extract useful information. To do this, we fit the xz -profile of the membrane by the ground state of the Helfrich model with periodic boundary conditions, which is one of the Euler buckling profiles of an elastic beam [28, 29]. This shape depends only on the dimensionless buckling parameter γ ($\gamma = 1$ is the flat state). Hence, if one period of the buckling profile for $L_x = 1$ is given by a parameter curve $x = s + \xi(s, \gamma), z = \zeta(s, \gamma)$ parameterized by a normalized arclength variable $0 < s < 1$, the general case $L_x \neq 1$ can be obtained by shifting and scaling.

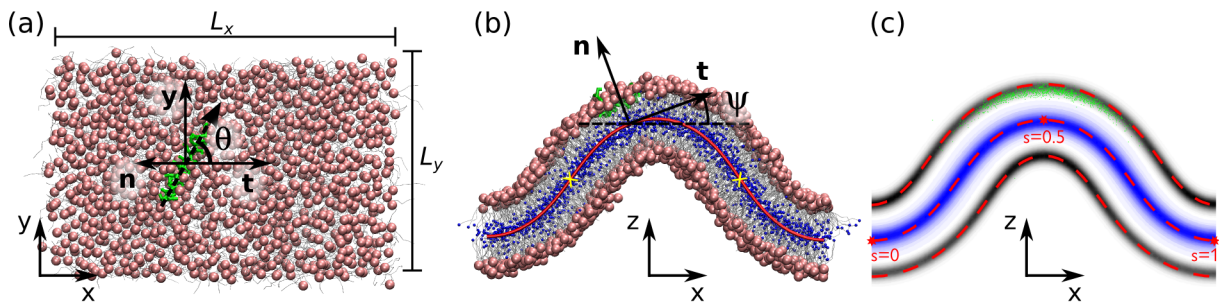


FIG. 2. (Color online) Buckled simulation and analysis. (a,b) Top and side view of a simulation snapshot. Lipids (gray), except phosphate groups (light red) and the inner lipid tail beads (blue), and the peptide (LL-37 in this case) in green. The system size is $L_x = 20.88$ nm and $L_y = 13.05$ nm. (a) The peptide orientation θ is the angle between the α -helical part (dashed arrow, pointing towards the C-terminal end) and the midplane tangent vector \mathbf{t} , in the midplane tangent plane. (b) The side view also shows the membrane mid-plane tangent (\mathbf{t}) and normal (\mathbf{n}) vectors, translated to the peptide center of mass for clarity, the tangent angle ψ , the Euler buckling profile (red line) fitted to the bilayer mid-plane, and the inflection points at $s = 0.5 \pm 0.25$ (yellow crosses) used to align the buckled configurations. Molecular graphics generated with VMD [34]. (c) Average buckled shape in terms of densities of inner lipid tail beads (blue) and phosphate groups (gray). Green dots show representative peptide center-of-mass positions. Dashed red lines indicate the average fitted mid-plane ± 2.15 nm offsets in the normal direction.

For fast evaluation, we expanded $\xi(s, \gamma)$ and $\zeta(s, \gamma)$ in truncated Fourier series in s , and created look-up tables for Fourier coefficients vs. γ . We defined s to give the curve $z(x)$ a maximum at $s = 0.5$, minima at $s = 0, 1$, and inflection points at $s = 0.5 \pm 0.25$ (see Fig. 2c), and aligned the buckled shapes by fitting the bilayer in each frame to the buckling profile and aligning the inflection points (Fig. 2b, movies S2-S3). Specifically, we fit the buckling profile to the innermost tail beads of all lipids in each frame using least-squares in the x and z directions, i.e., minimizing

$$\sum_i (x_0 + L_x(s + \xi(s_i, \gamma)) - x_i)^2 + (z_0 + L_x\zeta(s_i, \gamma) - z_i)^2 \quad (1)$$

with respect to γ , the translations x_0, z_0 , and the projected arc-length coordinates s_i of each bead (x_i, z_i are bead positions). The time-averaged bilayer shape, after aligning the mid-plane inflection points, agree well with the theoretical buckled shape (Fig. 2c).

The arclength position s of the peptide was computed by projecting the peptide center of mass onto the buckled profile fitted to the membrane midplane in every frame (Fig. 2b). The in-plane orientation θ was computed as follows: we fitted a line through the backbone particles of the alpha-helical part of the peptide, projected this line to the tangent plane defined by the midplane tangent vector \mathbf{t} and the \mathbf{y} unit vector, and took θ to be the angle between the projected line and \mathbf{t} . The local curvature is given by $C(s) = \frac{1-\gamma}{L_x} \frac{d\psi}{ds}$, where ψ is the bilayer mid-plane tangent angle (see Fig. 2b), and we neglect small shape and area fluctuations ($\text{std}(\gamma) \approx 0.005$), and use the nominal value $\gamma = 0.2$.

d. Fitting We used least-squares routines in MATLAB (MathWorks, Natick, MA) to fit the Boltzmann distributions $e^{-E(s_i, \theta_i)}/Z$ of the E_C (Eq. 7) and E_2 (Ta-

ble S1) models to (s, θ) -histograms built from the aggregated data with 50 bins for each coordinate. Both data and model histograms were normalized numerically. Error bars in Fig. 4d are boot-strap standard deviations from 1000 bootstrap realizations, using blocks of length 100 (500 ns) as the elementary data unit for resampling [49].

RESULTS

e. Preferred curvature and orientations We simulated single peptides interacting with a buckled bilayer, using three independent production runs of 15 μs for each peptide, and tracked their normalized arc-length coordinates $s \in [0, 1]$ and in-plane orientations θ (Fig. 2a). Aggregated (s, θ) -histograms are shown in Fig. 3a-c, and convergence is discussed in Sec. S1.

All three peptides prefer the concave high curvature regions with a maximum at $s = 0.5$, as expected for hydrophobic insertion mechanisms [15, 16, 30, 37, 50]. Regarding the angle distributions, the three peptides behave differently. Magainin displays a rather uniform angle distribution, probably because its short α -helical segment creates a fairly symmetric insertion footprint. For melittin, the joint between the N- and C-terminal helices appears very flexible, resulting in a broad distribution of the internal angle β (Fig. 3e). Both helices prefer directions nearly parallel to the x -axis, the direction of maximum curvature, but the preference is stronger and slightly offset ($\theta_{max} \approx -15^\circ, 165^\circ$) for the C-terminal helix shown in Fig. 3b, while the N-terminal helix is more symmetrically oriented (Fig. S2).

LL-37 maintains a linear structure, and its θ -distribution displays two sharp maxima near $\theta = 70^\circ$ and $\theta = -110^\circ$ (Fig. 3c). This is remarkable since, by

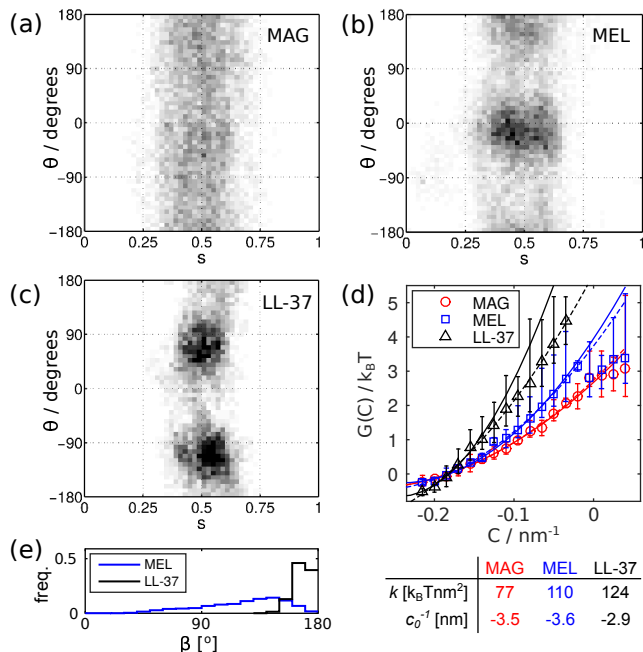


FIG. 3. (Color online) Distributions of peptide positions and orientations in a buckled bilayer for (a) magainin, (b) melittin (using the orientation of the C-terminal helix), and (c) LL-37. (d) Binding free energy vs. mean curvature at the peptide center-of-mass (Eq. (3)) for the three peptides. Error bars show max and min values from three independent simulations, solid lines are fits to the E_C model (Eq. (7)) discussed below, and dashed lines are fits to quadratic curves of the form $G(C) = \frac{k}{2}(C - c_0)^2 + \text{const.}$ (e) Distributions of internal angle (see Fig. 1) for melittin and LL-37.

reflection symmetry around $s = 0.5$, the curvatures in those directions are the same as along -70° and 110° , orientations that are clearly not preferred. As we will argue below, this can be understood as curvature sensing along directions different from that of the peptide itself. These sensing directions adopt $\theta = 0, 90^\circ$, and thus map onto themselves under reflection. Notably, none of the peptides orient directly along the flat direction $\theta = 90^\circ$ as commonly assumed in mechanical models [15, 16].

f. Orientation-averaged binding free energy Next, we look at the orientation-averaged binding free energy, corresponding to the curvature-dependent enrichment measured in many *in vitro* assays [17–23]. To extract the curvature dependence of the binding energy, we analyze center-of-mass positions along the buckled shape. These should follow a Boltzmann distribution, proportional to $e^{-G(s)}$, where $G(s)$ is the orientation-averaged binding free energy in units of $k_B T$.

We model this as depending on the local curvature only, and hence set $G(s) = G(C(s))$, and extract $G(C)$ from curvature histograms, weighted according to the change-of-variable transformation that relates the density of curvatures, $\rho(C)$, to the density of positions $\rho(s)$.

Indeed, dropping normalization constants, we have

$$\rho_s(s)ds \propto e^{-G(C(s))}ds \propto e^{-G(C)}|dC/ds|^{-1}dC \propto \rho_C(C)dC, \quad (2)$$

from which it follows that

$$G(C) = -\ln(\rho_C(C)|dC/ds|) + \text{const.} \quad (3)$$

The weights $|dC/ds|$ can be understood as compensating for the fact that not all curvatures have equal arclength footprints along the buckled profile. To estimate $G(C)$, we estimated $\rho(C)$ using a simple histogram, and the weights as the mean of $|dC/ds|$ for all contributions to each bin.

Fig. 3d shows the binding free energy profiles $G(C)$ for the different peptides, which are more similar than the θ, s distributions. All curves are well fit by quadratic curves that extrapolate to preferred curvature radii slightly above the monolayer thickness of about 2.2 nm, relevant to the inside of membrane pores. Magainin and melittin show clearly convex $G(C)$ profiles, but that of LL-37 is closer to linear. For comparison, experimental binding free energies of these peptides to flat membranes with anionic lipids range from -15 to $-10 k_B T$ [51].

g. Quantitative models We now turn to quantitative models of the peptides' curvature sensing. Generally, if the principal curvatures and directions are $c_{1,2}$ and $\vec{e}_{1,2}$, the curvature tensor, or second fundamental form, in a frame rotated by an in-plane angle θ relative to \vec{e}_1 , is given by

$$C_{ij} = \begin{bmatrix} C_{\parallel} & C_X \\ C_X & C_{\perp} \end{bmatrix} = \begin{bmatrix} H+D \cos 2\theta & D \sin 2\theta \\ D \sin 2\theta & H-D \cos 2\theta \end{bmatrix}, \quad (4)$$

where $H = (c_1 + c_2)/2$ and $D = (c_1 - c_2)/2$ are the mean and deviatoric curvatures, and \parallel, \perp denote the longitudinal and transverse directions of a peptide. Note the symmetry under rotations by 180° , since the curvature of a line is the same in both directions. For our buckled surface, $c_1 = C(s)$, $c_2 = 0$, and $\vec{e}_{1,2} = \vec{e}_{x,y}$.

The simplest models are linear in C_{ij} [5], but can be ruled out since they cannot reproduce the convex binding free energies in Fig. 3d. To see this, we write a general linear model in the form $E_1 = aH + bD \cos(2(\theta - \alpha))$, and integrate out the angular dependence to get

$$G_1 = -\ln \int_0^{2\pi} e^{-E_1} d\theta = aH - \ln I_0(bD) + \text{const.} \quad (5)$$

Since $H = D = C(s)/2$ on the buckled surface, and the modified Bessel function I_0 is convex, G_1 will be either convex (if $b \neq 0$) or direction insensitive (when $b \rightarrow 0$), in disagreement with Fig. 3d.

Moving on to quadratic terms, Akabori and Santangelo [10] explored a model of the form

$$E_X = \frac{k_{\parallel}}{2}(C_{\parallel} - C_{\parallel 0})^2 + k_X(C_X - C_{X0})^2 + \frac{k_{\perp}}{2}(C_{\perp} - C_{\perp 0})^2, \quad (6)$$

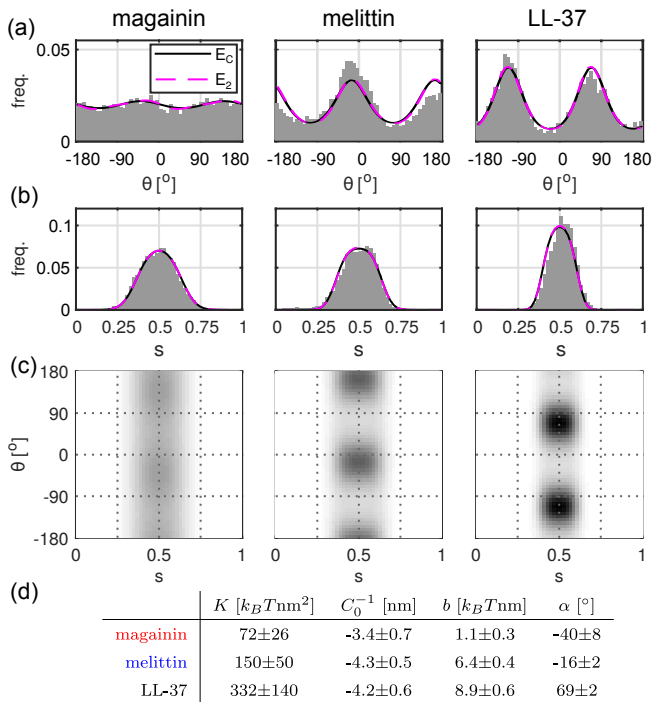


FIG. 4. (Color online) Fitting quadratic models to data. (a,b) marginal position and angle distributions, showing data (gray) and nearly identical curves from the E_C and general quadratic model (E_2 , see Table S1). (c) (s, θ) -distributions from fits to the E_C model of Eq. (7), (d) E_C fit parameters \pm bootstrap SEM [49] due to finite sampling (see Sec. S1), with α indicating the preferred orientation. Note that $E_C = \frac{K}{2}(C - C_0)^2$ in the isotropic limit $b = 0$, explaining the agreement between K, C_0 and k, c_0 of Fig. 3 for magainin.

where $C_{\parallel 0}, C_{X0}$ and $C_{\perp 0}$ are preferred curvatures. Further simplifications $k_X = 0$ and $k_X = k_{\perp} = 0$ have also been studied [6–9]. While these models can all display non-trivial behavior, E_X is not the most general quadratic model, which would include all 9 linear and quadratic combinations of the three independent curvature tensor components. In particular, E_X does not contain a simple preferred mean curvature as a special case, because $H = (C_{\parallel} + C_{\perp})/2$, and hence $(H - H_0)^2$ contains a term $C_{\parallel}C_{\perp}$ which is absent in Eq. (6).

However, the general quadratic model is not identifiable on surfaces with only one non-zero principal curvature. This is because the Gaussian curvature $c_1 c_2 = C_{\parallel}C_{\perp} - C_X^2$ vanishes, and hence the model can only be specified up to a term $\propto (C_{\parallel}C_{\perp} - C_X^2)$. Also, E_X can then be made to behave as a mean curvature sensor, since all angular dependence cancels if $k_{\parallel} = k_{\perp} = k_X, C_{\parallel 0} = C_{\perp 0}$, and $C_{X0} = 0$. These limitations apply to our buckled surface, as well as to tubular and plane-wave geometries used experimentally [17, 18, 21–23]. A curvature sensing mechanism therefore cannot be completely characterized using such surfaces, but some conclusions can be drawn.

In particular, setting $k_X = 0$ in Eq. (6) yields an in-

tuitive model with curvature sensing only along the longitudinal and transverse directions [6–9]. From Eq. (4), this means angular dependence only in the form $\cos 2\theta$, which is symmetric around $\theta = 0, \pm \frac{\pi}{2}$, and $\pm \pi$. However, the orientational distributions in Fig. 4a do not display this symmetry, although the statistics is not quite clear in the case of melittin (see Fig. S2). Apparently, the curvature sensing directions are not generally aligned with the actual helices. This resembles results for α -synuclein, where peptides and induced membrane deformations appear similarly misaligned [52].

A simple model incorporating these observations is

$$E_C = \frac{K}{2}(2H - C_0)^2 + bD \cos(2(\theta - \alpha)). \quad (7)$$

As shown in Fig. 4, E_C describes all peptides reasonably well, and using the full quadratic model does not significantly improve the fit. However, E_C is not uniquely determined due to the absence of Gaussian curvature, and we therefore explore alternative formulations with different physical interpretations. First, using Eq. (4) to trade H, D for the C_{ij} , and then the fact that $C_{\parallel}C_{\perp} = C_X^2$ (since the Gaussian curvature is zero in our simulations), we find that a model on the form of E_X ,

$$E'_C = \frac{K}{2}(C_{\parallel} - C_0 + \frac{b}{2K} \cos 2\alpha)^2 + K(C_X + \frac{b}{2K} \sin 2\alpha)^2 + \frac{K}{2}(C_{\perp} - C_0 - \frac{b}{2K} \cos 2\alpha)^2, \quad (8)$$

makes identical predictions as E_C on a buckled surface. Continuing, we can rotate the basis attached to the peptide by α , and thus generate a transformed curvature tensor with elements $C_{ij}^{(\alpha)}(\theta) = C_{ij}(\theta + \alpha)$ satisfying

$$C_{\parallel}^{(\alpha)} + C_{\perp}^{(\alpha)} = 2H, \quad C_{\parallel}^{(\alpha)} - C_{\perp}^{(\alpha)} = 2D \cos(2(\theta - \alpha)). \quad (9)$$

In this basis, there is an E_X -like equivalent model that lacks 'off-diagonal' elements,

$$E''_C = \frac{K}{2}(C_{\parallel}^{(\alpha)} - C_0 + \frac{b}{2K})^2 + \frac{K}{2}(C_{\perp}^{(\alpha)} - C_0 - \frac{b}{2K})^2, \quad (10)$$

i.e., sensing curvature along two orthogonal directions that are rotated with respect to the peptide backbone. Thus, there are some interesting possibilities that might be resolved by varying the Gaussian curvature.

As a consistency check, we integrated out θ from E_C . Proceeding as for G_1 in Eq. (5) and setting $H = D = C(s)/2$, we get

$$G_C = -\ln \int_0^{2\pi} d\theta e^{-E_C} = \frac{K}{2}(C - C_0)^2 - \ln I_0(bC/2), \quad (11)$$

which we compare with $G(C)$ in Fig. 3d using the parameters of Fig. 4d. Magainin and melittin shows good agreement, but not LL-37, whose (s, θ) -distribution (Fig. 3c) is also less symmetric around $s = 0.5$ than expected from

the symmetry of the buckled shape. Numerical experiments in Sec. S2 show that both symmetry and consistency improves when tracking the C-terminal helix instead, indicating that this part dominates the curvature sensing.

DISCUSSION

We describe a novel simulation approach to study membrane curvature sensing by tracking positions and orientations of single molecules interacting with a buckled lipid bilayer. This approach is widely applicable, and the utility of angular information is obvious from the observation that the three peptides show distinct orientational distributions, but very similar orientation-averaged binding energy curves (Fig. 3). These results should motivate efforts to track the position and orientation of membrane proteins experimentally, for example using polarization-based optical techniques [53] or electron microscopy [54]. Generalizations to more complex surface shapes, or possibly combinations of cylindrical and spherical shapes, in order to probe Gaussian curvature sensing would also be valuable.

Our data is well described by modeling the binding energy in terms of local curvatures, yielding more complex models than earlier fits to orientation-averaged data [17–20], and also less symmetric than some theoretical suggestions [6–9]. The observed asymmetry also seems difficult to reconcile with current mesoscopic models of hydrophobic insertion in terms of cylindrical membrane inclusions [15, 16]. Indeed, the mirror symmetry of cylindrical inclusions is absent both in the peptide structures and our data, which can instead be described in terms

of curvature sensing directions that are not aligned with the alpha-helical structures. Since amphipatic helices are common curvature sensing motifs [14] and mirror symmetry is generally absent also in multimeric proteins [55], such asymmetric sensing might be common.

Our results also have biophysical implications. At high concentrations, the three peptides are thought to mediate the formation of membrane pores with highly curved inner surfaces [47, 56, 57], and the orientational preferences we see in single peptides are consistent with atomistic[56] and coarse-grained[58] simulations of multi-peptide pores. The asymmetric curvature preference of LL-37 should help select for a single handedness of the resulting tilted pore structure [58], which might facilitate pore formation by reducing frustration. This mechanism may represent a general way for membrane proteins to induce a particular orientation or handedness in patterns on curved surfaces [59].

h. Acknowledgments We thank Astrid Gräslund, Oksana V. Manyuhina and Christoph A. Hazelwandter for helpful comments and discussions. Simulations were performed on resources provided by the Swedish National Infrastructure for Computing (SNIC) at the National Supercomputer Centre (NSC) and the High Performance Computing Center North (HPC2N). Financial support from the Wenner-Gren Foundations and the Swedish Foundation for Strategic Research (SSF) via the Center for Biomembrane Research are gratefully acknowledged.

i. Author contributions JG and ML designed research. JG and FEW performed research. JG and ML analyzed data. JG, FEW, and ML wrote the paper.

j. Conflict of interest none declared.

k. Supporting citations Ref. [60] appears in the Supporting Material.

-
- [1] J. Zimmerberg and M. M. Kozlov, *Nat. Rev. Mol. Cell Bio.* **7**, 9 (2006).
- [2] T. Baumgart, B. R. Capraro, C. Zhu, and S. L. Das, *Annu. Rev. Phys. Chem.* **62**, 483 (2011).
- [3] A. Tonnesen, S. M. Christensen, V. Tkach, and D. Stamou, *Biophys. J.* **106**, 201 (2014).
- [4] D. Engelman, *Nature* **438**, 578 (2005).
- [5] J. B. Fournier, *Phys. Rev. Lett.* **76**, 4436 (1996).
- [6] Š. Perutková, V. Kralj-Iglič, M. Frank, and A. Iglič, *J Biomech* **43**, 1612 (2010).
- [7] N. Ramakrishnan, P. B. Sunil Kumar, and J. H. Ipsen, *Phys. Rev. E* **81**, 041922 (2010).
- [8] N. Ramakrishnan, P. B. S. Kumar, and J. H. Ipsen, *Macromol. Theor. Simul.* **20**, 446 (2011).
- [9] N. Ramakrishnan, P. B. Sunil Kumar, and J. H. Ipsen, *Biophys. J.* **104**, 1018 (2013).
- [10] K. Akabori and C. D. Santangelo, *Phys. Rev. E* **84**, 061909 (2011).
- [11] N. Walani, J. Torres, and A. Agrawal, *Phys. Rev. E* **89**, 062715 (2014).
- [12] B. J. Peter, H. M. Kent, I. G. Mills, Y. Vallis, P. J. G. Butler, P. R. Evans, and H. T. McMahon, *Science* **303**, 495 (2004).
- [13] P. D. Blood and G. A. Voth, *Proc. Natl. Acad. Sci. U.S.A.* **103**, 15068 (2006).
- [14] G. Drin, J.-F. Casella, R. Gautier, T. Boehmer, T. U. Schwartz, and B. Antonny, *Nat. Struct. Mol. Biol.* **14**, 138 (2007).
- [15] F. Campelo, H. T. McMahon, and M. M. Kozlov, *Biophys. J.* **95**, 2325 (2008).
- [16] F. Campelo and M. M. Kozlov, *PLoS Comput. Biol.* **10**, e1003556 (2014).
- [17] C. Zhu, S. L. Das, and T. Baumgart, *Biophys. J.* **102**, 1837 (2012).
- [18] B. Sorre, A. Callan-Jones, J. Manzi, B. Goud, J. Prost, P. Bassereau, and A. Roux, *Proc. Natl. Acad. Sci. U.S.A.* **109**, 173 (2012).
- [19] S. Aimon, A. Callan-Jones, A. Berthaud, M. Pinot, G. E. S. Toombes, and P. Bassereau, *Dev. Cell* **28**, 212 (2014).
- [20] Z. Shi and T. Baumgart, *Nat. Commun.* **6**, 5974 (2015).
- [21] W.-T. Hsieh, C.-J. Hsu, B. R. Capraro, T. Wu, C.-M. Chen, S. Yang, and T. Baumgart, *Langmuir* **28**, 12838 (2012).

- [22] P. Ramesh, Y. F. Baroji, S. N. S. Reihani, D. Stamou, L. B. Oddershede, and P. M. Bendix, *Sci. Rep.* **3**, 1565 (2013).
- [23] J. C. Black, P. P. Cheney, T. Campbell, and M. K. Knowles, *Soft Matter* **10**, 2016 (2014).
- [24] M. N. Melo, R. Ferre, and M. A. R. B. Castanho, *Nat. Rev. Microbiol.* **7**, 245 (2009).
- [25] M. Zasloff, *Proc. Natl. Acad. Sci. U.S.A.* **84**, 5449 (1987).
- [26] E. Habermann, *Science* **177**, 314 (1972).
- [27] G. H. Gudmundsson, B. Agerberth, J. Odeberg, T. Bergman, B. Olsson, and R. Salcedo, *Eur. J. Biochem.* **238**, 325 (1996).
- [28] H. Noguchi, *Phys. Rev. E* **83**, 061919 (2011).
- [29] M. Hu, P. Diggins, and M. Deserno, *J. Chem. Phys.* **138**, 214110 (2013).
- [30] H. Cui, E. Lyman, and G. A. Voth, *Biophys. J.* **100**, 1271 (2011).
- [31] G. Wang, *J. Biol. Chem.* **283**, 32637 (2008), pDB: 2K6O.
- [32] T. Hara, H. Kodama, M. Kondo, K. Wakamatsu, A. Takeda, T. Tachi, and K. Matsuzaki, *Biopolymers* **58**, 437 (2001), PDB: 1DUM.
- [33] T. C. Terwilliger, L. Weissman, and D. Eisenberg, *Biophys. J.* **37**, 353 (1982), pDB: 2MLT.
- [34] W. Humphrey, A. Dalke, and K. Schulten, *J. Mol. Graphics* **14**, 33 (1996).
- [35] S. J. Marrink, H. J. Risselada, S. Yefimov, D. P. Tieleman, and A. H. de Vries, *J. Phys. Chem. B* **111**, 7812 (2007).
- [36] N. S. Hatzakis, V. K. Bhatia, J. Larsen, K. L. Madsen, P. Bolinger, A. H. Kunding, J. Castillo, U. Gether, P. Hedegård, and D. Stamou, *Nat. Chem. Biol.* **5**, 835 (2009).
- [37] S. Vanni, H. Hirose, H. Barelli, B. Antonny, and R. Gautier, *Nat. Commun.* **5**, 4916 (2014).
- [38] S. Pronk, S. Páll, R. Schulz, P. Larsson, P. Bjelkmar, R. Apostolov, M. R. Shirts, J. C. Smith, P. M. Kasson, D. van der Spoel, B. Hess, and E. Lindahl, *Bioinformatics* **29**, 845 (2013).
- [39] L. Monticelli, S. K. Kandasamy, X. Periole, R. G. Larson, D. P. Tieleman, and S.-J. Marrink, *J. Chem. Theory Comput.* **4**, 819 (2008).
- [40] S. O. Yesylevskyy, L. V. Schäfer, D. Sengupta, and S. J. Marrink, *PLoS Comput. Biol.* **6**, e1000810 (2010).
- [41] S. J. Marrink, A. H. de Vries, and A. E. Mark, *J. Phys. Chem. B* **108**, 750 (2004).
- [42] S. Baoukina, L. Monticelli, M. Amrein, and D. P. Tieleman, *Biophys. J.* **93**, 3775 (2007).
- [43] D. H. de Jong, G. Singh, W. F. D. Bennett, C. Arnarez, T. A. Wassenaar, L. V. Schäfer, X. Periole, D. P. Tieleman, and S. J. Marrink, *J. Chem. Theory Comput.* **9**, 687 (2013).
- [44] G. Bussi, D. Donadio, and M. Parrinello, *J. Chem. Phys.* **126**, 014101 (2007).
- [45] H. J. C. Berendsen, J. P. M. Postma, W. F. van Gunsteren, A. DiNola, and J. R. Haak, *J. Chem. Phys.* **81**, 3684 (1984).
- [46] U. Essmann, L. Perera, M. L. Berkowitz, T. Darden, H. Lee, and L. G. Pedersen, *J. Chem. Phys.* **103**, 8577 (1995).
- [47] M.-T. Lee, T.-L. Sun, W.-C. Hung, and H. W. Huang, *Proc. Natl. Acad. Sci. U.S.A.* **110**, 14243 (2013).
- [48] G. Wang, B. Mishra, R. F. Epand, and R. M. Epand, *BBA - Biomembranes Interfacially active peptides and proteins*, **1838**, 2160 (2014).
- [49] H. R. Künsch, *Ann. Stat.* **17**, 1217 (1989).
- [50] N. S. Hatzakis, V. K. Bhatia, J. Larsen, K. L. Madsen, P.-Y. Bolinger, A. H. Kunding, J. Castillo, U. Gether, P. Hedegård, and D. Stamou, *Nat. Chem. Biol.* **5**, 835 (2009).
- [51] Y. He and T. Lazaridis, *PLoS ONE* **8**, e66440 (2013).
- [52] A. R. Braun, E. Sevcik, P. Chin, E. Rhoades, S. Tristram-Nagle, and J. N. Sachs, *J. Am. Chem. Soc.* **134**, 2613 (2012).
- [53] S. A. Rosenberg, M. E. Quinlan, J. N. Forkey, and Y. E. Goldman, *Acc. Chem. Res.* **38**, 583 (2005).
- [54] K. M. Davies, C. Anselmi, I. Wittig, J. D. Faraldo-Gómez, and W. Kühlbrandt, *Proc. Natl. Acad. Sci. U.S.A.* **19**, 13602 (2012).
- [55] D. S. Goodsell and A. J. Olson, *Annu. Rev. Biophys. Biomol. Struct.* **29**, 105 (2000).
- [56] H. Leontiadou, A. E. Mark, and S. J. Marrink, *J. Am. Chem. Soc.* **128**, 12156 (2006).
- [57] K. A. Henzler Wildman, D.-K. Lee, and A. Ramamoorthy, *Biochemistry* **42**, 6545 (2003).
- [58] D. Sun, J. Forsman, and C. E. Woodward, *Langmuir* **31**, 752 (2015).
- [59] C. Mim, H. Cui, J. A. Gawronski-Salerno, A. Frost, E. Lyman, G. A. Voth, and V. M. Unger, *Cell* **149**, 137 (2012).
- [60] C. Ge, J. Gómez-Llobregat, M. J. Skwark, J.-M. Ruyschaert, Å. Wieslander, and M. Lindén, *FEBS J.* **281**, 3667 (2014).

**ANISOTROPIC MEMBRANE CURVATURE SENSING BY ANTIBACTERIAL PEPTIDES
– SUPPORTING INFORMATION.**

S1. CONVERGENCE AND INDIVIDUAL REPLICAS

Simulations of proteins interacting with mixed bilayers can be challenging to converge due to slow lipid diffusion and long-lived protein-lipid interactions [60]. For this reason, we run three independent replicas rather than one long simulation for each peptide, and use them as a simple control of the robustness of our conclusions. Figures S1-S3 show histograms of center-of-mass positions, orientations, and joint positions-orientations of both the three individual production runs for each peptide, as well as aggregated histograms. In the case of melittin (Fig. S2), orientations of both the N- and C-terminal helices are shown.

While the results for individual trajectories are obviously noisier than the aggregated statistics, it is clear that the same qualitative features are present in all replicas. In particular, two well-separated orientational states of melittin and LL-37 are clearly visible (albeit not equally populated) in all trajectories, strongly indicating that our simulations are long enough to capture the major low-energy states of these systems. However, the sampling is still limited enough to induce significant statistical uncertainty in fit parameters, as seen Fig. 4d.

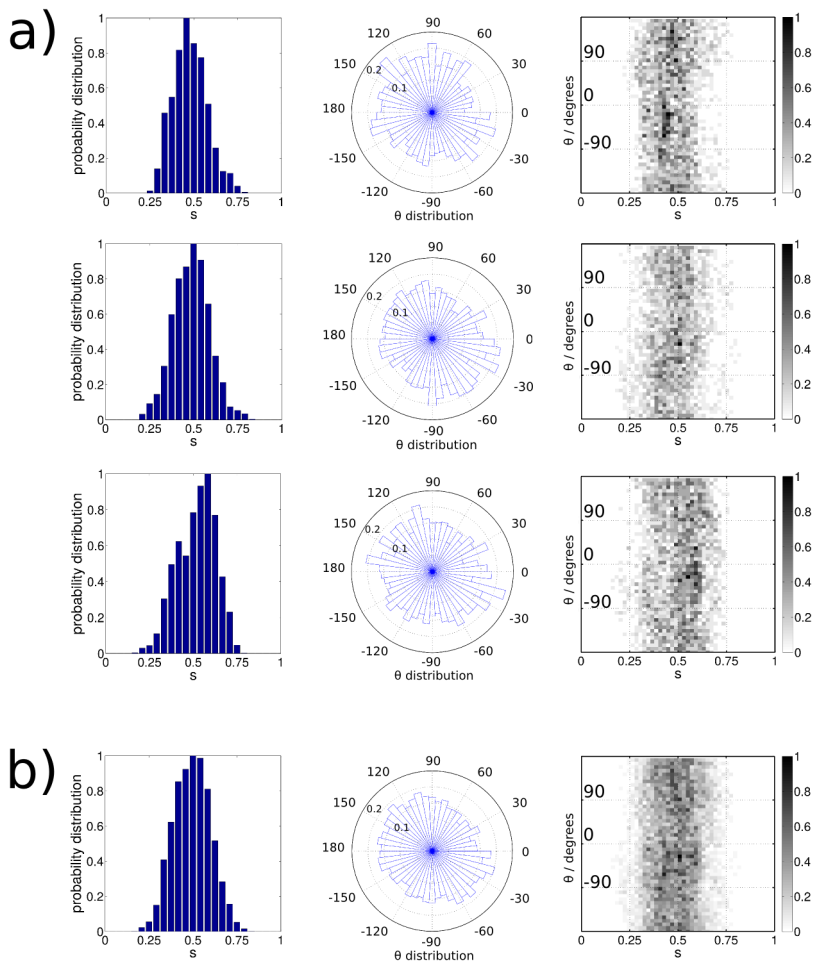


FIG. S1. Results for magainin, from (a) three independent production runs, and (b) aggregated.

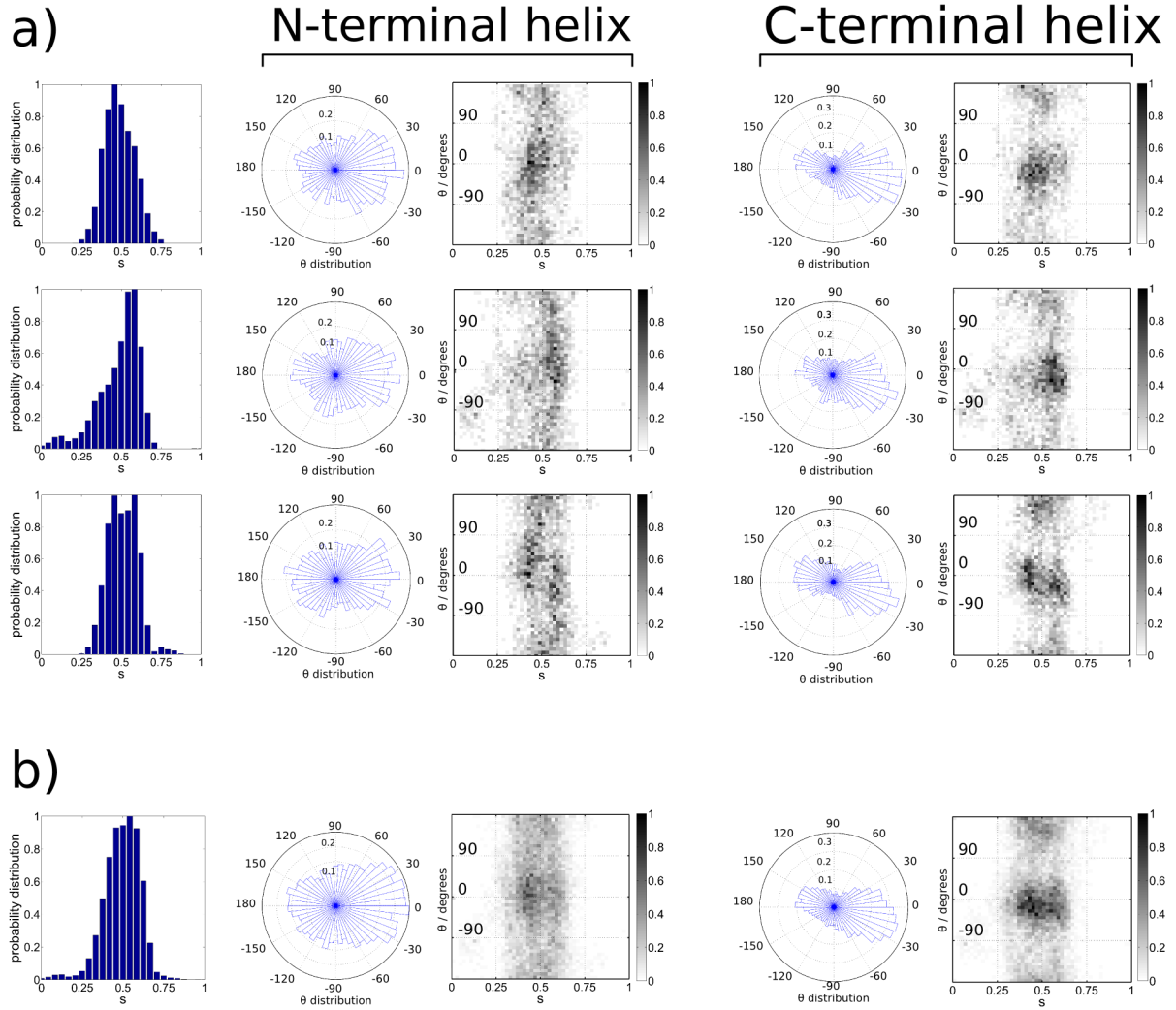


FIG. S2. Results for melittin, from (a) the three independent production runs, and (b) aggregated. Both N- and C-terminal results are shown.

TABLE S1. Fit parameters for the E_2 model for the curved shown in Fig. 4, rounded to two significant digits, in appropriate units of $K_B T$ and nm. This model is given by $E_2 = a_1 C_{\parallel}^2 + a_2 C_{\perp}^2 + a_3 C_X^2 + a_4 C_{\parallel} + a_5 C_{\perp} + a_6 C_X + a_7 C_X C_{\parallel} + a_8 C_X C_{\perp}$, i.e., with the $C_{\parallel} C_{\perp}$ term omitted for identifiability.

	a_1	a_2	a_3	a_4	a_5	a_6	a_7	a_8
magainin	36	34	73	21	21	-3.5	-9.2	-15
melittin	85	45	130	39	26	-0.52	15	12
LL-37	149	155	300	71	79	13	34	33

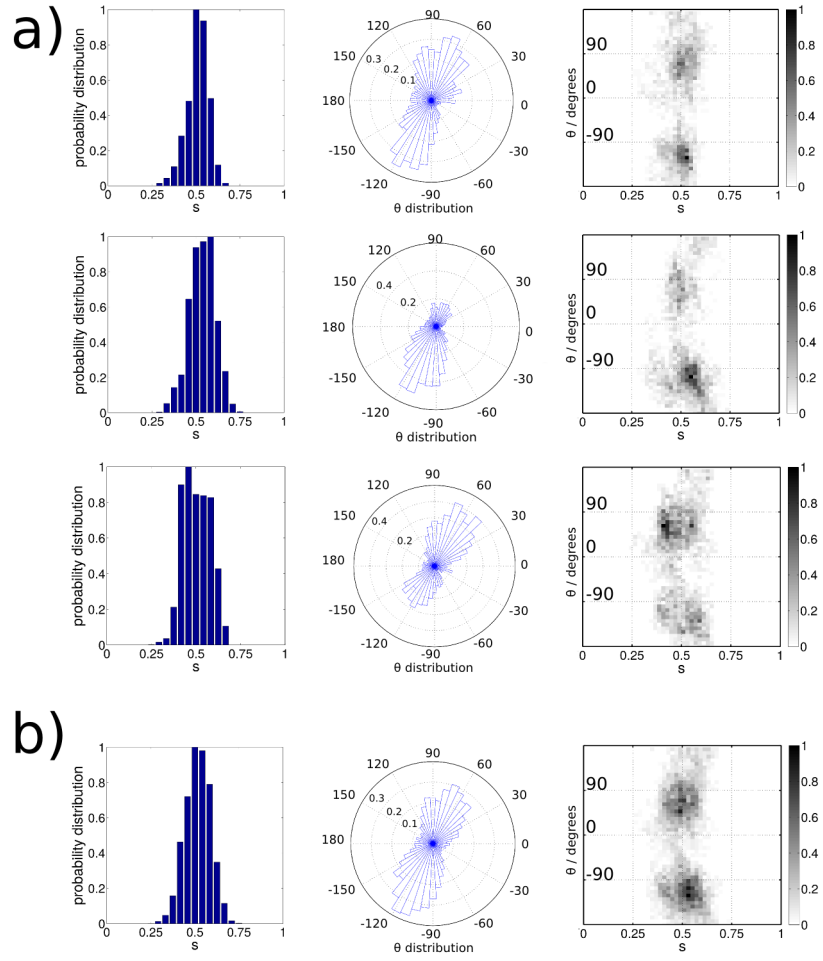


FIG. S3. Results for LL-37, from (a) three independent production runs, and (b) aggregated.

S2. LOCATION OF THE CURVATURE SENSING SITE ON LL-37

LL-37 shows indications of asymmetry around $s = 0.5$ that is incompatible with the symmetry of the curvature tensor elements (Fig. 3c), and the fitted E_C model is also less consistent with the orientation averaged binding energy (Fig. 3d) than the other peptides. Here, we explore the hypothesis that these effects are caused by using the center-of-mass of the peptide for defining the position s , which might be inappropriate if the sensitivity is unequally distributed along the peptide. Our rationale for this hypothesis is that a correlation between position and orientation, as indicated in the LL-37 data in Fig. 3c might come about if the effective curvature sensing site is different than the center-of-mass which we tracked to extract that data.

In Fig. S4, we show the corresponding analysis for LL-37 assuming a few alternative effective curvature sensing sites, with the center-of-mass in the middle row. The correlation between θ and s in each peak clearly becomes more pronounced when the tracking site moves towards the N-terminal end. However, the asymmetry almost disappears when one assumes the effective curvature sensing site to be the center of mass of the C-terminal helix, and appears again with the opposite trend when tracking the C-terminal end. Of these cases, the center-of-mass of the C-terminal helix is most consistent with the symmetries of curvature tensor elements, which indicates that this part of the peptide is more important for curvature sensing. Fitting the E_C model to this data yields $K = 323 \pm 127 \text{ k}_B\text{Tnm}^2$, $C_0^{-1} = -4.1 \pm 0.5 \text{ nm}$, $b = 0.2 \pm 0.3 \text{ k}_B\text{Tnm}$, and $\alpha = 69 \pm 2^\circ$, not significantly different from the parameters shown in Fig. 4.

However, all distributions are still slightly asymmetric around $s = 0.5$, with average s -values ranging from about 0.52 to 0.51 for the N- and C-terminal ends respectively, corresponding to an average displacement of 0.5 nm to 0.35 nm from the mid point. A closer examination of the significance of this observation would require substantially better statistics, perhaps from using some enhanced sampling method, as well as more systematic studies using a larger range of curvatures. This is outside the scope of this study.

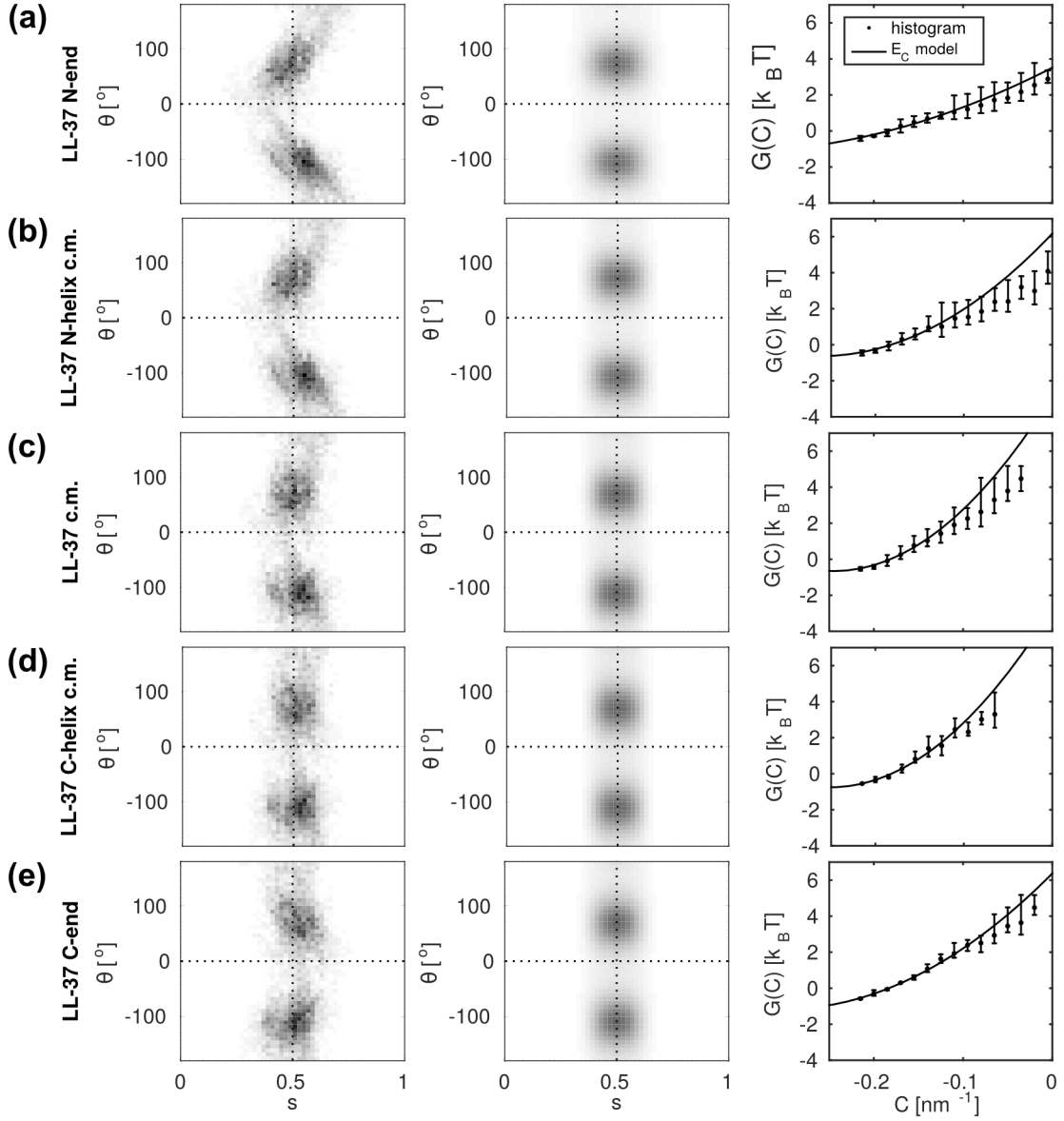


FIG. S4. Analysis of LL-37 using different definitions of s and θ , namely (a) the first residue and orientation of the N-terminal helix, (b) the center-of-mass and orientation of the N-terminal helix, (c) the center-of-mass and orientation of the whole peptide (same as shown in the main text), (d) the center-of-mass and orientation of the C-terminal helix, and (e) the last residue and orientation of the C-terminal helix. relevant curvature sensing site. The columns show (left) the (s, θ) -histogram, (mid) a fit of the E_C model, and (right) the orientation-averaged binding free energy, obtained from the model fit (line) or using weighted histograms, Eq. 3, (dots) with error bars as in Fig. 3. The fit and histogram curves are vertically aligned by least-squares fit of the points at $C \leq -0.15 \text{ nm}^{-1}$.